Radial basis function method for a multidimensional linear elliptic equation with nonlocal boundary conditions

Svajūnas Sajavičius*

Department of Computer Science II, Faculty of Mathematics and Informatics, Vilnius University, Naugarduko str. 24, LT-03225 Vilnius, Lithuania

Department of Mathematical Modelling, Faculty of Economics and Finance Management, Mykolas Romeris University, Ateities str. 20, LT-08303 Vilnius, Lithuania

Abstract

The development of numerical methods for the solution of partial differential equations (PDEs) with nonlocal boundary conditions is important, since such type of problems arise as mathematical models of various real-world processes. We use radial basis function (RBF) collocation technique for the solution of a multidimensional linear elliptic equation with classical Dirichlet boundary condition and nonlocal integral conditions. RBF-based meshless methods are easily implemented and efficient, especially for multidimensional problems formulated on complexly shaped domains. In this paper, properties of the method are investigated by studying two- and three-dimensional test examples with manufactured solutions. We analyze the influence of the RBF shape parameter and the distribution of the nodes on the accuracy of the method as well as the influence of nonlocal conditions on the conditioning of the collocation matrix.

Keywords: multidimensional elliptic equation, nonlocal integral condition, meshless method, radial basis function, collocation

1. Introduction

Elliptic partial differential equations (PDEs) have important applications in various areas of mathematics and physics. For example, the Laplace equation arises in modeling various kinds of conservative physical systems in equilibrium, and the Poisson equation has many applications in electrostatics, mechanical engineering and theoretical physics. The Helmholtz equation appears in mathematical models related to steady-state oscillations in mechanics, acoustics, electromagnetics etc. In mathematical modeling, elliptic PDEs are used together with boundary conditions specifying the solution on the boundary of the domain. Dirichlet, Neumann and Cauchy conditions are examples of classical boundary conditions. In some cases, classical boundary conditions cannot describe process or phenomenon precisely. Therefore, mathematical models of various physical, chemical, biological or environmental processes often involve nonclassical conditions. Such conditions usually are identified as *nonlocal (boundary) conditions* and reflect situations when the data on the domain boundary cannot be measured directly, or when the data on the boundary

*Correspondence address: Department of Computer Science II, Faculty of Mathematics and Informatics, Vilnius University, Naugarduko str. 24, LT-03225 Vilnius, Lithuania. Tel.: +370 5 2193091; fax: +370 5 2151585.

Email address: svajunas.sajavicius@mif.vu.lt svajunas@mruni.eu (Svajūnas Sajavičius)

URL: http://www.mif.vu.lt/~svajunas (Svajūnas Sajavičius)

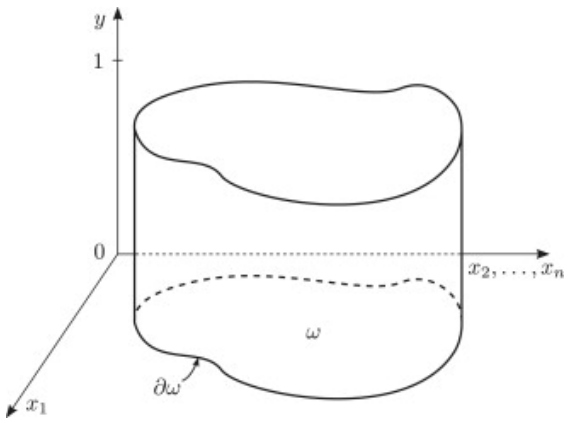

Figure 1: Sketch of the domain Ω.

depend on the data inside the domain. For example, we can mention problems in thermoelasticity [1], thermodynamics [2], hydrodynamics [3] or plasma physics [4].

We consider a multidimensional linear elliptic equation

$$\mathcal{L}[u] := -\frac{\partial^2 u}{\partial y^2} - \sum_{i,j=1}^{n} \frac{\partial}{\partial x_i}\Big(a_{ij}\frac{\partial u}{\partial x_j}\Big) + a_0 u = f \quad \text{in } \Omega = \omega \times (0,1), \tag{1}$$

subject to classical Dirichlet boundary condition

$$u = 0 \quad \text{on } \partial\omega \times (0,1), \tag{2}$$

and nonlocal integral conditions

$$\int_0^{\xi_1} u(\mathbf{x}, y)\mathrm{d}y = 0, \quad \int_{\xi_2}^{1} u(\mathbf{x}, y)\mathrm{d}y = 0, \quad \mathbf{x} \in \omega, \tag{3}$$

where $\omega \subset \mathbb{R}^n$ ($n \geqslant 1$) is a bounded domain with Lipschitz boundary $\partial\omega$, $0 < \xi_1 < \xi_2 < 1$ and $f : \Omega \to \mathbb{R}$, $a_{ij}, a_0 : \omega \to \mathbb{R}$ are given functions from suitable spaces. The sketch of the cylindrical domain Ω is given in Fig. 1.

The existence and uniqueness results for this problem have been obtained by Avalishvili et al. [5, 6].

Theorem ([5, 6]). *If $f \in L^2(\Omega)$, the coefficients $a_{ij}, a_0 \in L^\infty(\omega)$ and satisfy the conditions*

$$a_0(\mathbf{x}) \geqslant 0, \quad a_{ij} = a_{ji},$$
$$\sum_{i,j=1}^{n} a_{ij}\xi_j\xi_i \geqslant c_a \sum_{i=1}^{n} |\xi_i|^2, \quad \forall \xi_i \in \mathbb{R}, \quad i, j = 1, 2, \ldots, n,$$

where c_a is a positive constant (see [5, 6]), then the problem (1)–(3) has a unique solution.

PDEs with nonlocal conditions and numerical methods for their solution are popular objectives of research. The finite difference schemes for two-dimensional elliptic problems with nonlocal boundary conditions have been considered in papers [3, 7–11]. In papers [12, 13], the solvability of the finite difference schemes for similar problems has been proved and the discretization error estimates have been obtained.

Some error estimates on the finite element approximation for two-dimensional elliptic problem with nonlocal boundary conditions are given in paper [14]. In paper [15], a high order composite scheme for the second order elliptic problem is presented and a fast algorithm for its solution is designed. A new constructive method for the solution of the two-dimensional Poisson equation with Bitsadze–Samarskii nonlocal boundary condition has been proposed [16]. Various finite difference schemes for the solution of multidimensional nonlocal elliptic boundary value problems have been studied in paper [17]. In papers [18, 19], stable finite difference schemes for the solution of multidimensional elliptic equations with multipoint nonlocal boundary conditions have been proposed and analyzed. However, in papers mentioned above, problems were formulated on regular domains and numerical experiments were performed only with two-dimensional test examples.

Traditional numerical techniques for the solution of PDEs (such as finite differences, finite volumes, finite elements etc.), are based on the domain discretization using meshes. For multidimensional problems formulated on complexly shaped domains, mesh generation can be very time consuming. Recently, meshless methods for the numerical solution of PDEs became popular between scientists and engineers [20, 21]. Such type of methods do not require mesh generation or remeshing.

The radial basis function (RBF) collocation methods is one class of meshless methods. RBFs successfully can be used both for the interpolation of scattered multidimensional data and for the numerical solution of PDEs [22–24]. The superiority of the RBF technique against the finite difference method [25], or finite difference and dual reciprocity methods [26], or finite difference and pseudospectral methods [27] already has been demonstrated. In paper [28] it has been demonstrated that the RBF collocation method for the solution of elliptic equations with classical boundary conditions is more accurate than the finite element method with the same mesh. Papers [27, 29–43] are dedicated especially to questions related to the solution of various elliptic problems with classical boundary conditions using RBF-based meshless methods.

The RBF-based meshless methods for the solution of PDEs with nonlocal boundary conditions have been applied in a few papers. We can mention works [44–47] where such methods where used for the solution of various time-dependent problems. In paper [48], the meshless method based on RBF collocation technique has been applied for the solution of the two-dimensional Poisson equation with nonlocal boundary condition formulated instead of classical boundary condition. The cases of nonlocal two-point and integral boundary conditions have been considered and the influence of these nonclassical boundary conditions on various properties of the method has been investigated by numerical study. The problem considered in paper [48] was formulated on a two-dimensional rectangular domain. However, the efficiency of the RBF-based meshless methods fully unfolds when they are used to solve multidimensional problems formulated on complexly shaped domains.

The present paper is dedicated to the solution of multidimensional elliptic problem (1)–(3). The meshless method based on RBF collocation technique is constructed and examined. The efficiency of the method is demonstrated by solving two- and three-dimensional test problems. The influence of the RBF shape parameter and the distribution of the nodes on the accuracy of the method as well as the influence of nonlocal conditions on the conditioning of the collocation matrix are investigated. To the best of our knowledge, this is the first time when a multidimensional elliptic PDE with nonlocal boundary conditions is solved using RBF-based meshless method.

The paper is organized as follows. In Section 2, the RBF-based meshless method for the considered multidimensional differential problem (1)–(3) is constructed. The results of numerical experiments with two- and three-dimensional test problems are presented and discussed in Section 3. Some remarks in Section 4 conclude the paper.

Table 1
Globally supported and infinitely smooth RBFs ($r = \|\mathbf{x}\|$).

RBF	Definition
Multiquadric (MQ)	$\phi(r) = \sqrt{1 + (\epsilon r)^2}$
Inverse Multiquadric (IMQ)	$\phi(r) = (\sqrt{1 + (\epsilon r)^2})^{-1}$
Inverse Quadric (IQ)	$\phi(r) = (1 + (\epsilon r)^2)^{-1}$
Gaussian (GA)	$\phi(r) = \exp(-(\epsilon r)^2)$

2. Construction of the method

2.1. Radial basis functions

First of all, let us recall some basic definitions and facts from the theory of RBFs [22, 23].

A multivariate real-valued function $\Phi : \mathbb{R}^d \to \mathbb{R}$ is called a *radial function* if there exists a univariate function $\phi : [0, \infty) \to \mathbb{R}$ such that

$$\Phi(\mathbf{x}) = \phi(\|\mathbf{x}\|),$$

where $\|\cdot\|$ is some norm on $\mathbb{R}^d$ (usually the Euclidean norm is used). Thus, the value $\Phi(\mathbf{x})$ depends only on the norm of vector $\mathbf{x}$.

In Table 1, some popular examples of globally supported and infinitely smooth RBFs are given. All these RBFs contain a free parameter $\epsilon > 0$ which is called the *shape parameter* and controls the shape of RBF. The same RBFs also can be expressed using the shape parameter $c = 1/\epsilon$. Then, for example, MQ and GA RBFs are generated by the functions ϕ defined as $\phi(r) = \sqrt{c^2 + r^2}$ and $\phi(r) = \exp(-(r/c)^2)$, respectively.

It is known [22, 23] that IMQ, IQ and GA RBFs are strictly positive definite and MQ RBF is conditionally positive definite of order one. In case of interpolation problem, the positive definiteness of RBF ensures the invertibility of the interpolation matrix. When conditionally positive definite RBFs are used, the non-singularity of the problem is ensured by augmenting the interpolant with a polynomial of the corresponding order and appending interpolation system by some homogeneous linear equations. However, singular cases are very rare and interpolation methods based on conditionally positive RBF are useful and efficient even without any augmentation of the interpolants.

2.2. Domain representation

In the present paper, $\mathbf{x} = [x_1, x_2, \ldots, x_n]^T \in \mathbb{R}^n$ is n-dimensional vector and we denote $(\mathbf{x}, y) = [x_1, x_2, \ldots, x_n, y]^T \in \mathbb{R}^{n+1}$.

The problem domain Ω and its boundary $\partial\Omega$ should be represented by a set of distinct *scattered nodes*. The domain of the problem (1)–(3) is cylindrical and for representation we use the method which reflects to this property. We represent the domain by parallel layers of nodes. These layers are allocated along the y-direction (see Fig. 2). Let

$$\Xi_{[0,1]} = \{y_1 = 0, y_2, y_3, \ldots, y_{N_1-1}, y_{N_1} = 1\} \subset [0, 1]$$

be a set of distinct nodes scattered on the interval $[0, 1]$, and $\Xi_{(0,1)} = \Xi_{[0,1]} \setminus \{y_1 = 0, y_{N_1} = 1\}$. Then, for each $y_k \in \Xi_{[0,1]}$ we generate two non-empty sets of nodes,

$$\Xi_{\omega}^{(k)} = \{\mathbf{x}_{k_{(l)}}\}_{l=1}^{N_2} \subset \omega, \quad \Xi_{\partial\omega}^{(k)} = \{\mathbf{x}_{k_{(l)}}\}_{l=1}^{N_3} \subset \partial\omega,$$

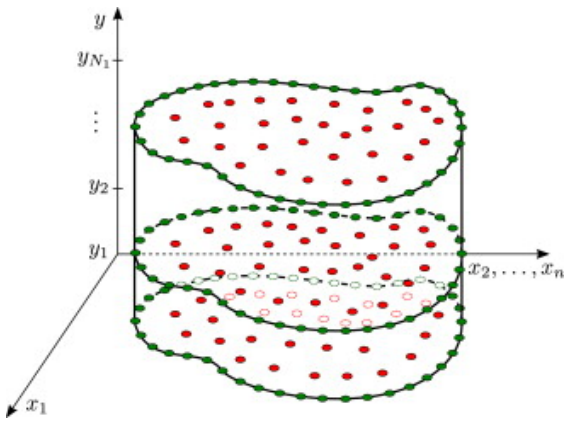

Figure 2: Representation of the domain Ω and its boundary $\partial\Omega$.

which represent the domain ω and its boundary $\partial\omega$. The sets $\Xi_{\partial\omega}^{(k)}$ and $\Xi_{\omega}^{(k)}$ can be the same or different for each k. For simplicity, we assume that N_2 and N_3 are fixed for every k.

Thus, the domain Ω and its boundary $\partial\Omega$ are represented by the set of distinct scattered nodes

$$\Xi = \bigcup_{y_k \in \Xi_{[0,1]}} (\Xi_{\partial\omega}^{(k)} \cup \Xi_{\omega}^{(k)}) \times \{y_k\} \subset \overline{\Omega}$$

with a total number of nodes $|\Xi| = N$ ($N = N_1 \cdot (N_2 + N_3)$). We assume that the nodes used for the domain representation coincide with the *centers* of RBF.

2.3. Collocation

Using standard RBF interpolation approach, we seek for an approximate solution to the problem (1)–(3) in the form

$$\overline{u}(\mathbf{x}, y) = \mathbf{\Phi}^T(\mathbf{x}, y)\boldsymbol{\lambda},$$

where

$$\mathbf{\Phi}(\mathbf{x}, y) = [\phi_1(\mathbf{x}, y), \phi_2(\mathbf{x}, y), \ldots, \phi_N(\mathbf{x}, y)]^T$$

and

$$\phi_k(\mathbf{x}, y) = \phi(\|(\mathbf{x}, y) - (\mathbf{x}_k, y_k)\|_2)$$

for a given RBF ϕ with center $(\mathbf{x}_k, y_k) \in \Xi$, $\|\cdot\|_2$ denotes the Euclidean norm, and $\boldsymbol{\lambda} = [\lambda_1, \lambda_2, \ldots, \lambda_N]^T$ are coefficients to be determined using collocation technique. By imposing approximate solution $\overline{u}(\mathbf{x}, y)$ to satisfy Eq. (1) on the nodes representing Ω we get the following linear equations:

$$\mathcal{L}[\mathbf{\Phi}^T](\mathbf{x}, y)\boldsymbol{\lambda} = f(\mathbf{x}, y), \quad (\mathbf{x}, y) \in \bigcup_{y_k \in \Xi_{(0,1)}} \Xi_{\omega}^{(k)} \times \{y_k\}. \tag{4}$$

From Dirichlet boundary condition (2) we obtain these equations:

$$\mathbf{\Phi}^T(\mathbf{x}, y)\boldsymbol{\lambda} = 0, \quad (\mathbf{x}, y) \in \bigcup_{y_k \in \Xi_{[0,1]}} \Xi_{\partial\omega}^{(k)} \times \{y_k\}. \tag{5}$$

Table 2
Expressions of definitely integrated (with respect to y) functions $\Phi(\mathbf{x}, y) = \phi(\|(\mathbf{x}, y)\|_2)$ with integration intervals $(0, \xi_1)$ (upper rows) and $(\xi_2, 1)$ (lower rows).

RBF	Integrated functions
MQ	$\frac{1}{2}\Big(\xi_1\sqrt{1+(\epsilon\|(\mathbf{x},\xi_1)\|_2)^2} + \frac{1+(\epsilon\|\mathbf{x}\|_2)^2}{\epsilon}\cdot\ln\Big(\frac{\epsilon\xi_1+\sqrt{1+(\epsilon\|(\mathbf{x},\xi_1)\|_2)^2}}{\sqrt{1+(\epsilon\|\mathbf{x}\|_2)^2}}\Big)\Big)$
	$-\frac{1}{2}\Big(\xi_2\sqrt{1+(\epsilon\|(\mathbf{x},\xi_2)\|_2)^2} + \frac{1+(\epsilon\|\mathbf{x}\|_2)^2}{\epsilon}\cdot\ln\Big(\frac{\epsilon\xi_2+\sqrt{1+(\epsilon\|(\mathbf{x},\xi_2)\|_2)^2}}{c+\sqrt{1+(\epsilon(\|(\mathbf{x},1)\|_2))^2}}\Big)\Big)$
IMQ	$\frac{1}{\epsilon}\ln\Big(\frac{\epsilon\xi_1+\sqrt{1+(\epsilon\|(\mathbf{x},\xi_1)\|_2)^2}}{\sqrt{1+(\epsilon\|\mathbf{x}\|_2)^2}}\Big)$
	$-\frac{1}{\epsilon}\ln\Big(\frac{\epsilon\xi_2+\sqrt{1+(\epsilon\|(\mathbf{x},\xi_2)\|_2)^2}}{c+\sqrt{1+(\epsilon\|(\mathbf{x},1)\|_2)^2}}\Big)$
IQ	$\frac{1}{\epsilon\sqrt{1+(\epsilon\|\mathbf{x}\|_2)^2}}\arctan\Big(\frac{\epsilon\xi_1}{\sqrt{1+(\epsilon\|\mathbf{x}\|_2)^2}}\Big)$
	$-\frac{1}{\epsilon\sqrt{1+(\epsilon\|\mathbf{x}\|_2)^2}}\Big(\arctan\Big(\frac{\epsilon\xi_2}{\sqrt{1+(\epsilon\|\mathbf{x}\|_2)^2}}\Big)-\arctan\Big(\frac{\epsilon}{\sqrt{1+(\epsilon\|\mathbf{x}\|_2)^2}}\Big)\Big)$
GA	$\frac{\sqrt{\pi}}{2\epsilon}\,\mathrm{erf}\,(\epsilon\xi_1)\exp\left(-(\epsilon\|\mathbf{x}\|_2)^2\right)$
	$-\frac{\sqrt{\pi}}{2\epsilon}(\mathrm{erf}\,(\epsilon\xi_2)-\mathrm{erf}\,(\epsilon))\exp\left(-(\epsilon\|\mathbf{x}\|_2)^2\right)$

Finally, nonlocal integral conditions (3) lead to the following linear equations:

$$\mathbf{I}_1^T(\mathbf{x})\boldsymbol{\lambda} = 0, \quad \mathbf{x}\in\Xi_\omega^{(1)}, \tag{6}$$

$$\mathbf{I}_2^T(\mathbf{x})\boldsymbol{\lambda} = 0, \quad \mathbf{x}\in\Xi_\omega^{(N_1)}, \tag{7}$$

where

$$\mathbf{I}_1(\mathbf{x}) = \int_0^{\xi_1}\boldsymbol{\Phi}(\mathbf{x},y)\mathrm{d}y = [I_{1,1}(\mathbf{x}), I_{1,2}(\mathbf{x}), \ldots, I_{1,N}(\mathbf{x})]^T,$$

$$\mathbf{I}_2(\mathbf{x}) = \int_{\xi_2}^{1}\boldsymbol{\Phi}(\mathbf{x},y)\mathrm{d}y = [I_{2,1}(\mathbf{x}), I_{2,2}(\mathbf{x}), \ldots, I_{2,N}(\mathbf{x})]^T,$$

and

$$I_{1,k}(\mathbf{x}) = \int_0^{\xi_1}\phi_k(\mathbf{x},y)\mathrm{d}y, \quad I_{2,k}(\mathbf{x}) = \int_{\xi_2}^{1}\phi_k(\mathbf{x},y)\mathrm{d}y.$$

For the functions ϕ given in Table 1, computing of $I_{1,k}(\mathbf{x})$ and $I_{2,k}(\mathbf{x})$ is not complicated and numerical integration is not required. In Table 2, the expressions of definitely integrated (with respect to y) functions $\Phi(\mathbf{x}, y) = \phi(\|(\mathbf{x}, y)\|_2)$ are given.

Thus, the collocation equations (4)–(7) form the linear system

$$\mathbf{A}\boldsymbol{\lambda} = \mathbf{b}. \tag{8}$$

If globally supported RBF is used, the collocation matrix $\mathbf{A}$ is dense (full) and it tends to be ill-conditioned, especially when $\epsilon \to 0$. Since for quite high accuracy the RBF-based methods require small values of the shape parameter ϵ, such methods cannot be very accurate and well-conditioned at the same time (this is known as *uncertainty* or *trade-off principle*, see [23, 49]).

In the following section we will examine our method by analyzing a couple of test examples.

3. Numerical study

3.1. Test examples

We demonstrate the efficiency of the considered method and analyze its properties by solving two- and three-dimensional test examples with manufactured solutions. In each example, the function $f \in L^2(\Omega)$ in Eq. (1) is chosen so that prescribed function u would be solution to the differential problem (1)–(3) formulated on particular domain Ω.

Two-dimensional example ($n = 1$). First of all, we consider two-dimensional differential problem formulated on the domain Ω with $\omega = (0, L)$. The coefficients of the equation (1) are $a_{11} \equiv 1$ and $a_0 \equiv 1$, i.e. we consider a special case of the Helmholtz equation

$$-\frac{\partial^2 u}{\partial y^2} - \frac{\partial^2 u}{\partial x_1^2} + u = f \quad \text{in } \Omega = \omega \times (0, 1).$$

The function $f \in L^2(\Omega)$ is set so that the exact solution of the problem is the function

$$u(x_1, y) = \sin\Big(\frac{2\pi x_1^2}{L^2}\Big) \cdot \nu(y; \xi),$$

where

$$\nu(y; \xi) = \frac{\pi\xi \sin(\pi y) + \cos(\pi\xi) - 1}{\pi\xi + \cos(\pi\xi) - 1}.$$

The function $u(x_1, y)$ satisfies Dirichlet boundary condition (2) and nonlocal integral conditions (3) with $\xi_1 = \xi$ and $\xi_2 = 1 - \xi$ ($0 < \xi < 1/2$). In our numerical study, ω was the unit interval ($L = 1$).

Three-dimensional example ($n = 2$). Three-dimensional test example is formulated on the domain Ω with

$$\omega = \{\mathbf{x} \in \mathbb{R}^2 : r_1 < \|\mathbf{x}\|_2 < r_2\}.$$

In this case, we consider equation

$$-\frac{\partial^2 u}{\partial y^2} - \frac{\partial^2 u}{\partial x_1^2} - \frac{\partial^2 u}{\partial x_2^2} + u = f \text{ in } \Omega = \omega \times (0, 1),$$

i.e. $a_{11} = a_{22} \equiv 1$, $a_{12} = a_{21} \equiv 0$ and $a_0 \equiv 1$. The function $f \in L^2(\Omega)$ is such that the exact solution of the problem is the function

$$u(x_1, x_2, y) = \sin\Big(\frac{\pi(\|\mathbf{x}\|_2 - r_1)}{r_2 - r_1}\Big) \cdot \nu(y; \xi).$$

Both Dirichlet boundary condition (2) and nonlocal integral conditions (3) with $\xi_1 = \xi$ and $\xi_2 = 1 - \xi$ ($0 < \xi < 1/2$) are satisfied. We used $r_1 = 0.5$ and $r_2 = 1$.

3.2. Nodes distribution

The geometrical flexibility is one of the most important advantages of the RBF-based meshless methods. Such methods are expected to work well when the problem domain is represented using scattered nodes.

In our numerical experiments with two- and three-dimensional examples, the interval $[0, 1]$ was represented by $N_1 = \widetilde{N}$ regularly (uniformly) distributed nodes, where $\widetilde{N}$ is arbitrary positive integer. In our study, the numbers of nodes representing the domain ω and its boundary $\partial\omega$ were equal to $N_2 = \widetilde{N} - 2$ and $N_3 = 2$ (two-dimensional example), or $N_2 = (\widetilde{N} - 2)\widetilde{N}$ and $N_3 = 2\widetilde{N}$ (three-dimensional example). Therefore, a total number of nodes $N = \widetilde{N}^2$ (two-dimensional example) or $N = \widetilde{N}^3$ (three-dimensional example). In two-dimensional example, the boundary $\partial\omega$ was represented by two nodes, while in three-dimensional example the boundary $\partial\omega$ consisted of two concentric circles. On each circle, nodes were distributed regularly (uniformly). The nodes representing the boundary $\partial\omega$ were fixed, while for the representation of the domain ω three different strategies were used.

Regular distribution. In one-dimensional example, the domain $\overline{\omega}$ is represented by equidistantly distributed nodes

$$\mathbf{x}_k = kL/(\widetilde{N} - 1),$$

$k = 1, 2, \ldots, \widetilde{N} - 2$. In two-dimensional example, nodes are distributed regularly on concentric circles:

$$\mathbf{x}_{k_{(l)}} = (\rho_k \cos\theta_l, \rho_k \sin\theta_l),$$

where $\rho_k = r_1 + k(r_2 - r_1)/(\widetilde{N} - 1)$, $k = 1, 2, \ldots, \widetilde{N} - 2$, and $\theta_l = 2\pi l/\widetilde{N}$, $l = 0, 1, \ldots, \widetilde{N} - 1$.

Perturbed distribution. Regularly distributed nodes are randomly perturbed. Therefore, the one-dimensional domain ω is represented by the nodes

$$\mathbf{x}_k = kL/(\widetilde{N} - 1) + \widetilde{x}_k,$$

where $\widetilde{x}_k$ are random numbers uniformly distributed on the interval $[-L/(2(\widetilde{N} - 1)), L/(2(\widetilde{N} - 1)))$, $k = 1, 2, \ldots, \widetilde{N}-2$. In three-dimensional example (when the domain $\overline{\omega}$ is two-dimensional), regularly distributed nodes are perturbed radially and angularly:

$$\mathbf{x}_{k_{(l)}} = ((\rho_k + \widetilde{\rho}_{k_{(l)}}) \cos(\theta_l + \widetilde{\theta}_{k_{(l)}}), (\rho_k + \widetilde{\rho}_{k_{(l)}}) \sin(\theta_l + \widetilde{\theta}_{k_{(l)}})),$$

where $\widetilde{\rho}_{k_{(l)}}$ and $\widetilde{\theta}_{k_{(l)}}$ are random numbers uniformly distributed on the intervals $[-(r_2 - r_1)/(2(\widetilde{N} - 1)), (r_2 - r_1)/(2(\widetilde{N} - 1)))$ and $[-\pi/\widetilde{N}, \pi/\widetilde{N})$, respectively, $k, l = 0, 1, \ldots, \widetilde{N} - 1$. Perturbed distribution usually is quite uniform (each node is located on its own sector).

Random distribution. The nodes representing the domain ω are selected randomly. In two-dimensional example, we set

$$\mathbf{x}_k = \widetilde{x}_k,$$

where $\widetilde{x}_k$ are random numbers uniformly distributed on the interval $[0, L)$, $k = 1, 2, \ldots, \widetilde{N} - 2$. The two-dimensional domain ω is represented by the following nodes:

$$\mathbf{x}_{k_{(l)}} = (\widetilde{\rho}_{k_{(l)}} \cos\widetilde{\theta}_{k_{(l)}}, \widetilde{\rho}_{k_{(l)}} \sin\widetilde{\theta}_{k_{(l)}}),$$

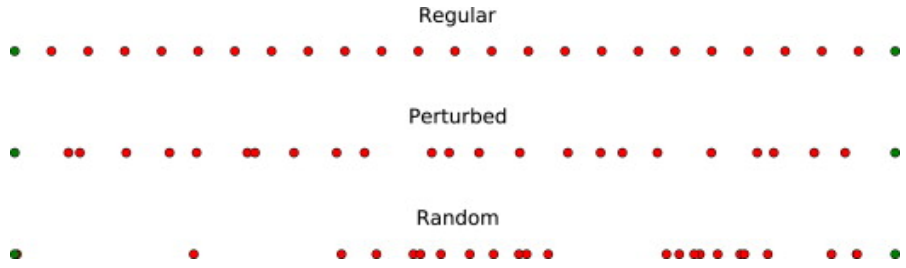

Figure 3: Representation of the domain $\overline{\omega}$ (two-dimensional example) by regular, perturbed and random distributions of nodes ($\widetilde{N} = 25$).

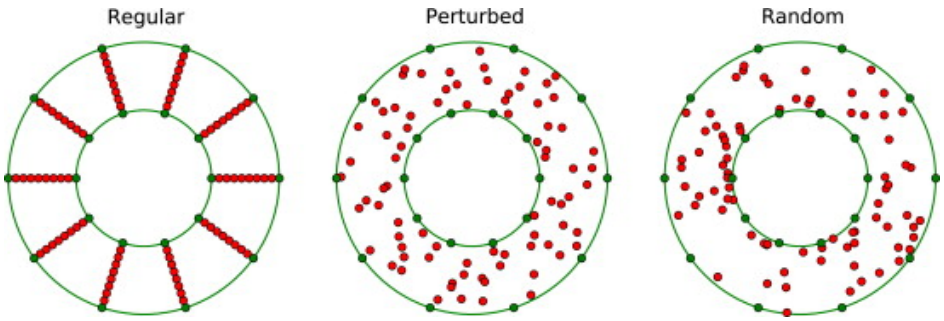

Figure 4: Representation of the domain $\overline{\omega}$ (three-dimensional example) by regular, perturbed and random distributions of nodes ($\widetilde{N} = 10$).

where $\widetilde{\rho}_{k_{(l)}}$ and $\widetilde{\theta}_{k_{(l)}}$ are random numbers uniformly distributed on the intervals $[r_1, r_2)$ and $[0, 2\pi)$, respectively, $k = 1, 2, \ldots, \widetilde{N} - 2$, $l = 0, 1, \ldots, \widetilde{N} - 1$.

Examples of different nodes distributions on the one- and two-dimensional domains $\overline{\omega}$ are depicted in Figs. 3 and 4, respectively. If a total number of nodes is relatively small, the perturbed and random distributions of nodes can be significantly different. The density of nodes can be estimated by the *fill distance* which is defined as

$$h = \sup_{(\mathbf{x},y)\in\Omega} \min_{(\mathbf{x}_k,y_k)\in\Xi} \|(\mathbf{x}, y) - (\mathbf{x}_k, y_k)\|_2.$$

The fill distance h together with the shape parameter ϵ affects the convergence rate and error estimates [50, 51]. Insufficiently dense distribution of the nodes can cause the increasing of the fill distance and the decreasing of the accuracy of the method. If the domain is represented by relatively large number of nodes, the perturbed and random representations are expected to be very similar and there should not be any significant difference between the results obtained using the same method with these two strategies of the domain representation.

3.3. Implementation of the method and measurement of its accuracy

The examined method has been implemented using Python programming language. For the solution of linear system (8), the standard routine `solve` from SciPy [52] subpackage linalg was used. SciPy package is built using the optimized ATLAS LAPACK and BLAS libraries [53].

The condition number of the matrix $\mathbf{A}$ was evaluated as the ratio of the largest and smallest singular values,

$$\kappa(\mathbf{A}) = \|\mathbf{A}\|_2 \|\mathbf{A}^{-1}\|_2 = \frac{\sigma_{\max}}{\sigma_{\min}}.$$

This ratio was computed using standard routines from SciPy package.

To estimate the accuracy of the solution obtained using the considered method, we computed N_e error

$$N_e = \sqrt{\frac{\sum_{(\mathbf{x},y)\in\Xi_{\text{test}}} (u(\mathbf{x},y) - \overline{u}(\mathbf{x},y))^2}{\sum_{(\mathbf{x},y)\in\Xi_{\text{test}}} u^2(\mathbf{x},y)}},$$

and the root mean square (RMS) error

$$E_{\text{RMS}} = \sqrt{\frac{1}{M} \sum_{(\mathbf{x},y)\in\Xi_{\text{test}}} (u(\mathbf{x},y) - \overline{u}(\mathbf{x},y))^2},$$

where $\Xi_{\text{test}} \subset \overline{\Omega}$ is a set of test points, $M = |\Xi_{\text{test}}|$. In the experiments with different nodes distributions, the accuracy was estimated on regularly distributed nodes.

Statistical analysis (descriptive statistics and hypotheses testing) have been done using SciPy subpackage STATS.

In this study, we examined efficiency of the method based on MQ RBF.

3.4. Results and discussion

3.4.1. Influence of the shape parameter

First of all, we solved our problems with various values of the shape parameter ϵ and regularly distributed nodes. In Fig. 5, we demonstrate how the accuracy of the method and the condition number $\kappa(\mathbf{A})$ depend on the shape parameter ϵ. As it is well-known, accurate results can be obtained if the shape parameter ϵ is selected successfully.

The optimal selection of the shape parameter is not completely understood yet. However, there exist some strategies for the optimization of the shape parameter [54–62]. The effectiveness of such strategies and other questions related to the optimal selection of RBF shape parameters very often are investigated by numerical experiments [38, 63–66]. The residual error also can be used as an error indicator which allows to optimize the selection of the shape parameter [63, 64].

By using the considered method we construct the closed-form approximate solution $\overline{u}(\mathbf{x},y)$ which is accurate not only on the collocation points but also on the whole domain $\omega \times (0,1)$. The absolute errors $|u(\mathbf{x},y) - \overline{u}(\mathbf{x},y)|$ obtained using the method with different nodes distribution are demonstrated in Figs. 6 and 7.

3.4.2. Conditioning of the collocation matrix

It is well-known that the collocation matrix $\mathbf{A}$ becomes ill-conditioned if the shape parameter ϵ is decreased. This complicates the solution of linear system (8). In papers [63, 64, 66, 67], the conditioning of the RBF-based methods for the interpolation and the solution of PDEs have been studied numerically. Recently, the stability estimates on the RBF-based meshless method for the Poisson equation with classical boundary conditions have been obtained in paper [68].

We investigated how the conditioning of the method depends on the parameters of nonlocal integral conditions (3). We solved our test examples with different values of ξ (assuming that $\xi_1 = \xi$ and $\xi_2 = 1 - \xi$) and evaluated the condition number of the matrix $\mathbf{A}$ together with the errors N_e and E_{RMS}. The distributions and number of nodes as well as the values of the shape parameter ϵ were fixed.

From Fig. 8 we see that the expansion of the integration interval does not have any negative influence on the conditioning of the method in both considered cases. Moreover, the condition number $\kappa(\mathbf{A})$ is slightly bigger when ξ is small, i.e., ξ_1 and ξ_2 are close to 0 and 1, respectively.

In further studies it would be interesting to investigate deeply the relationship between the conditioning of the considered method and the conditioning of the differential problem itself.

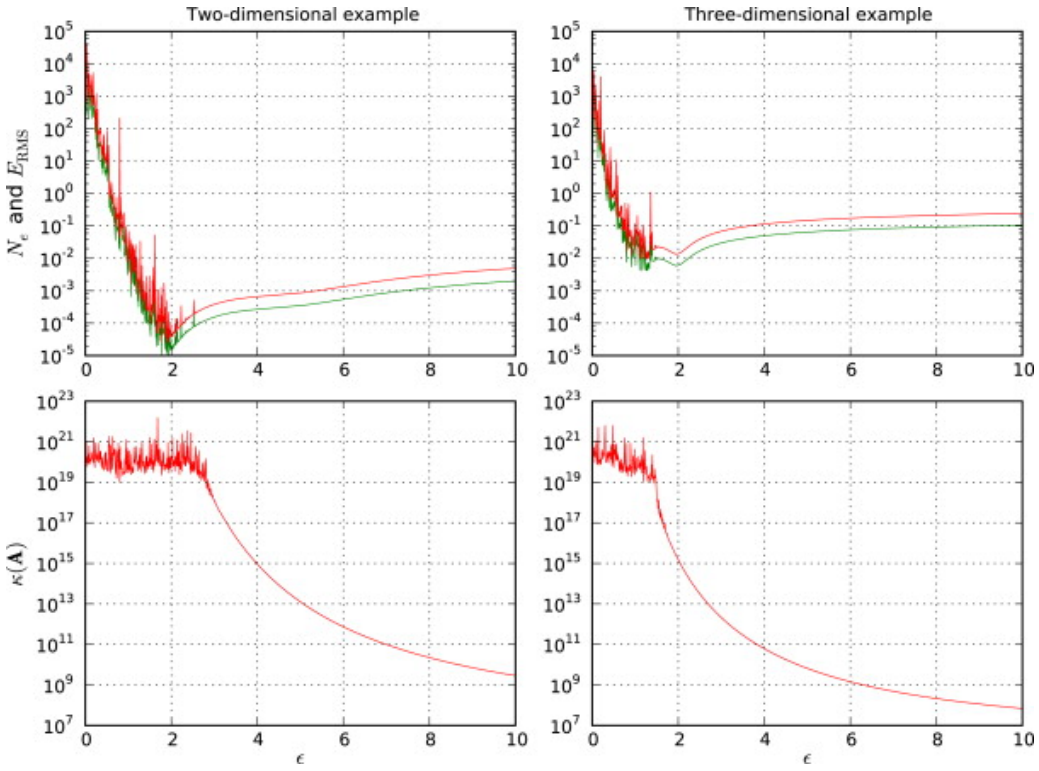

Figure 5: The dependence of the accuracy of the method (errors N_e and E_{RMS} are depicted as red curves and green curves, respectively) and the condition number $\kappa(\mathbf{A})$ on the values of the MQ RBF shape parameter ϵ: $\xi = 0.25$ ($\xi_1 = 0.25$, $\xi_2 = 0.75$); nodes were distributed regularly, $N = 625$ (in two-dimensional example) and $N = 1000$ (in three-dimensional example). (For interpretation of the references to color in this figure legend, the reader is referred to the web version of this article.)

3.4.3. Influence of the nodes distribution

We were interested whether the accuracy of the method with regularly distributed nodes significantly differs from the accuracy of the method with perturbed or randomly distributed nodes. We have compared errors N_e which arise when the method with regularly distributed nodes are used ($\varepsilon_{\mathrm{regular}}$) and means of errors N_e arising when the problem is solved using the method with perturbed or randomly distributed nodes (we denote these means as $\mu_{\mathrm{perturbed}}$ or μ_{random}, respectively). Moreover, it was interesting to compare the accuracy of results obtained using the method with perturbed and randomly distributed nodes.

The method was examined using 1000 perturbed and the same number of random representations of the domain. Therefore, two samples with 1000 real positive numbers (errors N_e) in each were analyzed. Descriptive statistics are presented in Table 3. The errors N_e obtained using the method with regular nodes distribution, minimal and maximal values of the errors, quartiles (Q_1, Q_2 and Q_3) as well as the means and standard deviations of the samples are reported. Moreover, the percentage of cases when the method with perturbed or random nodes distributions demonstrates more accurate results (smaller errors N_e) than the method with regular nodes distribution is presented. As we can see, there exist certain differences between the accuracy of the results obtained using the method with different nodes distributions. Very often the perturbed nodes distributions lead to more accurate results than the regular nodes distributions. Random distributions seem to be less effective and in certain unsuccessful cases such distributions can decrease the accuracy very drastically (the maximal errors N_e obtained when both test examples were solved using random nodes distributions are very high).

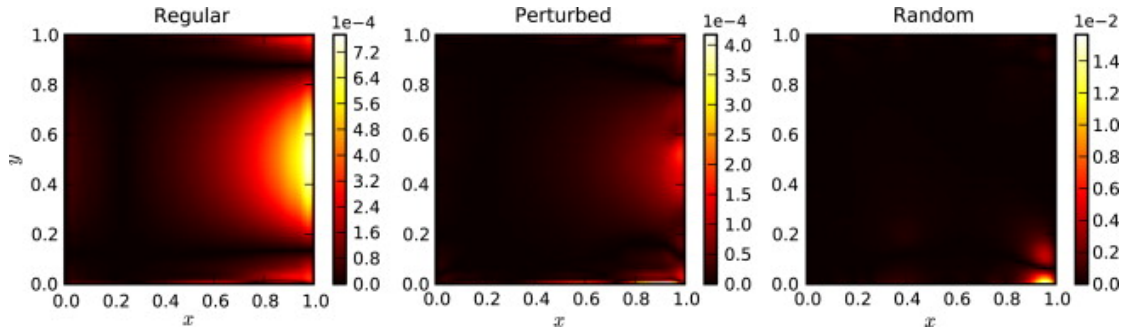

Figure 6: The absolute errors $|u(\mathbf{x}, y) - \overline{u}(\mathbf{x}, y)|$ obtained using the method with different nodes distributions: two-dimensional example, $\xi = 0.25$ ($\xi_1 = 0.25$, $\xi_2 = 0.75$), $\epsilon = 3.0$; $N = 625$.

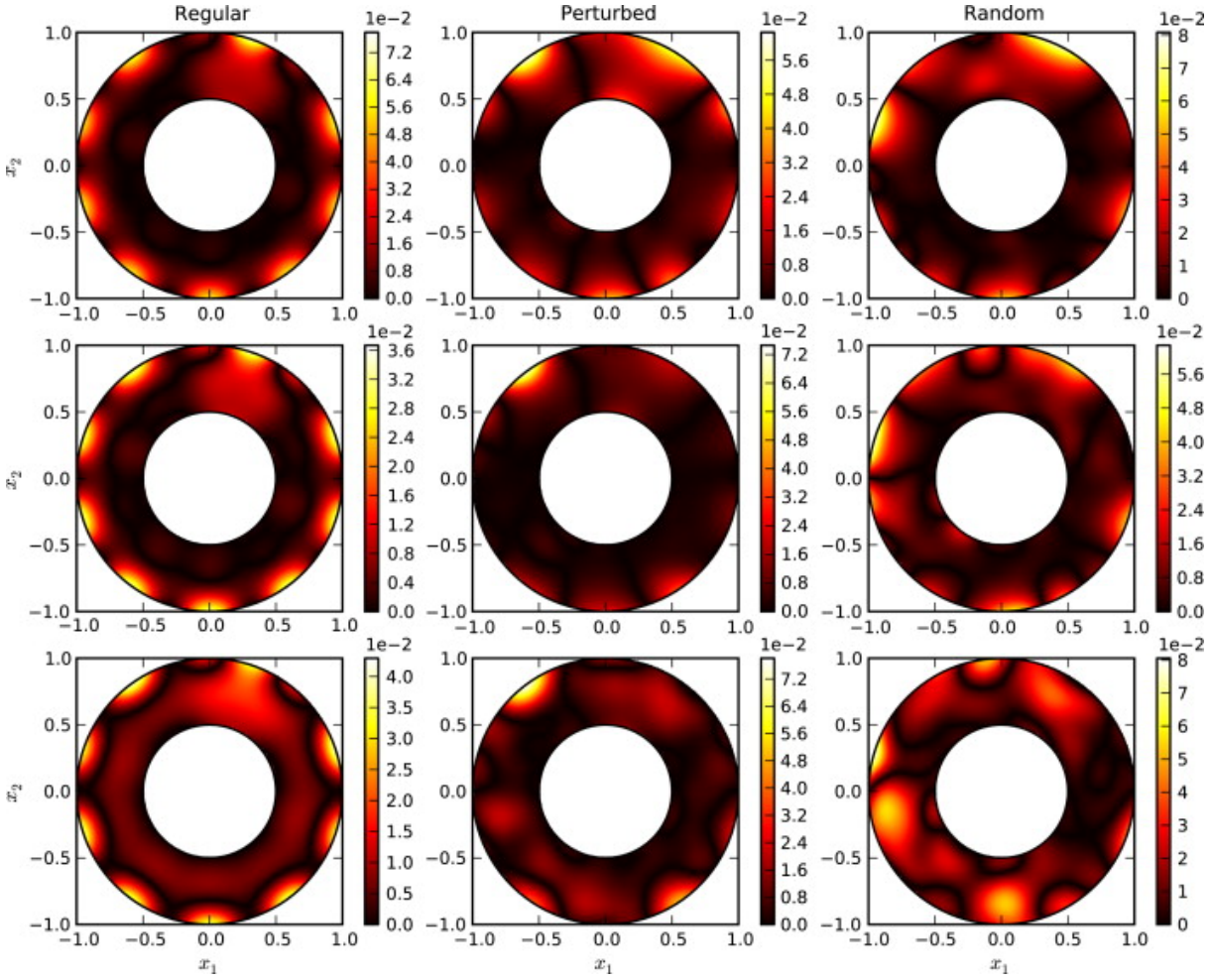

Figure 7: The absolute errors $|u(\mathbf{x}, y) - \overline{u}(\mathbf{x}, y)|$ obtained using the method with different nodes distributions: three-dimensional example, $\xi = 0.25$ ($\xi_1 = 0.25$, $\xi_2 = 0.75$), $\epsilon = 1.75$; $N = 1000$; $y = 0.0$ (bottom), $y = 0.25$ (middle) and $y = 0.5$ (top).

In order to estimate the statistical significance of differences between the errors obtained using the

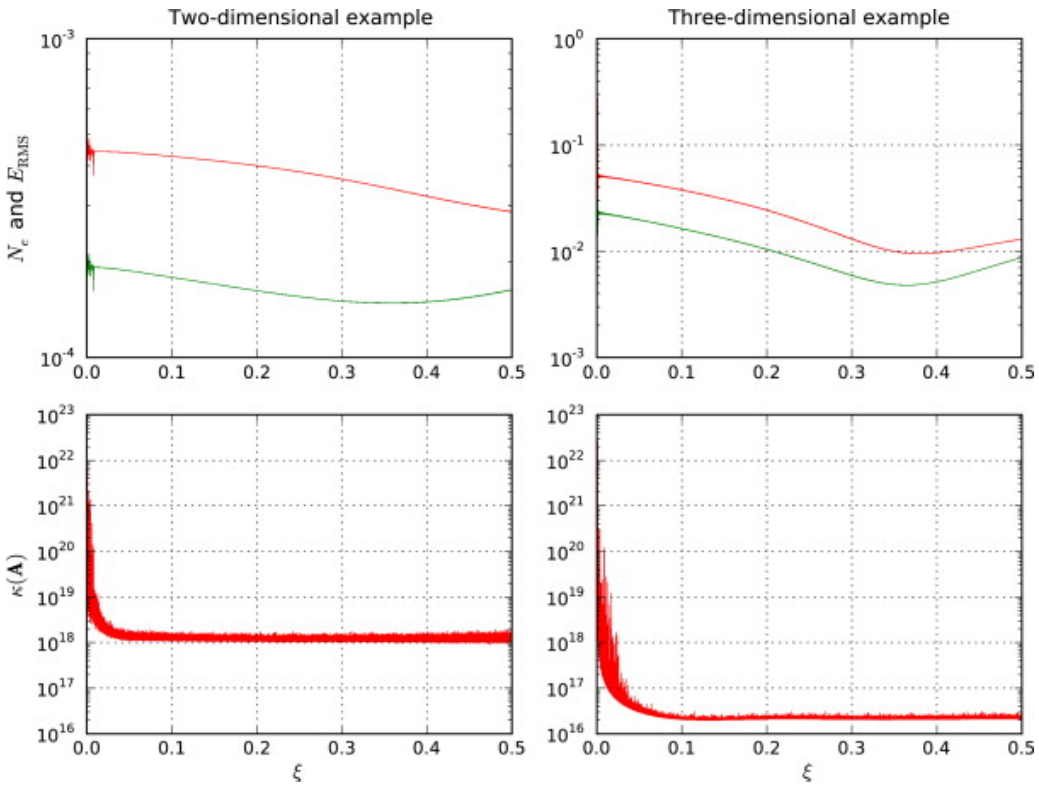

Figure 8: The dependence of the accuracy of the method (errors N_e and E_{RMS} are depicted as red curves and green curves, respectively) and the condition number $\kappa(\mathbf{A})$ on the values of ξ ($\xi_1 = \xi$, $\xi_2 = 1 - \xi$); $\epsilon = 3.0$ (two-dimensional example) and $\epsilon = 1.75$ (three-dimensional example); nodes were distributed regularly, $N = 625$ (in two-dimensional example) and $N = 1000$ (in three-dimensional example). (For interpretation of the references to color in this figure legend, the reader is referred to the web version of this article.)

method with different nodes distributions, we have tested the following statistical hypotheses:

$$\begin{cases} H_0 : \mu_{\text{perturbed}} = \varepsilon_{\text{regular}}, \\ H_1 : \mu_{\text{perturbed}} \neq \varepsilon_{\text{regular}}; \end{cases} \tag{H_{A}}$$

$$\begin{cases} H_0 : \mu_{\text{random}} = \varepsilon_{\text{regular}}, \\ H_1 : \mu_{\text{random}} \neq \varepsilon_{\text{regular}}; \end{cases} \tag{H_{B}}$$

$$\begin{cases} H_0 : \mu_{\text{perturbed}} = \mu_{\text{random}}, \\ H_1 : \mu_{\text{perturbed}} \neq \mu_{\text{random}}. \end{cases} \tag{H_{C}}$$

One-sample t-test was conducted to test the hypotheses (H_{A}) and (H_{B}) (to compare the accuracy of the method with regular and perturbed, or regular and random nodes distributions), and two-sample t-test was conducted in order to test the hypothesis (H_{C}) (to compare the accuracy of the method with perturbed and randomly distributed nodes). The results given in Table 4 (t-statistics and p-values) suggest the following conclusions:

- We did not detect any statistically significant differences between the accuracy of the results obtained using the method with regular and perturbed distributions of nodes.

Table 3
The errors N_e obtained using the method with regularly distributed nodes and descriptive statistics of samples of the errors N_e obtained using the method with 1000 different perturbed or random distributions of nodes: $\xi = 0.25$ ($\xi_1 = 0.25$, $\xi_2 = 0.75$); $\epsilon = 3.0$ (two-dimensional example) and $\epsilon = 1.75$ (three-dimensional example); number of nodes $N = 625$ (two-dimensional example), $N = 1000$ (three-dimensional example).

	Two-dimensional example	Three-dimensional example
Regular distribution		
N_e	$3.8251629473777928 \times 10^{-4}$	$1.8211269206325688 \times 10^{-2}$
Perturbed distribution		
Min.	$1.0564313810748669 \times 10^{-4}$	$6.6505795889404808 \times 10^{-3}$
Q_1	$1.2961593246900498 \times 10^{-4}$	$9.9576260474105189 \times 10^{-3}$
Q_2 (median)	$1.4235688625701418 \times 10^{-4}$	$1.2512355991517442 \times 10^{-2}$
Q_3	$1.7109563462663292 \times 10^{-4}$	$1.7091598440315155 \times 10^{-2}$
Max.	$3.3498859544301745 \times 10^{0}$	$7.2046929384332459 \times 10^{-1}$
Mean	$3.6507990358546679 \times 10^{-3}$	$1.8244767288817708 \times 10^{-2}$
Standard deviation	$1.0587627211348517 \times 10^{-1}$	$3.6127338830293468 \times 10^{-2}$
Percentage of better cases	93.1	77.6
Random distribution		
Min.	$1.3189636926819095 \times 10^{-4}$	$9.1374269181689581 \times 10^{-3}$
Q_1	$4.8276122352070965 \times 10^{-4}$	$1.8347033663356150 \times 10^{-2}$
Q_2 (median)	$1.1350670174968339 \times 10^{-3}$	$2.6794201802338061 \times 10^{-2}$
Q_3	$3.4191010310099302 \times 10^{-3}$	$4.2570338028627940 \times 10^{-2}$
Max.	$1.7467967762382813 \times 10^{1}$	$5.1457766812486145 \times 10^{0}$
Mean	$2.7059641358826821 \times 10^{-2}$	$6.9473490787397396 \times 10^{-2}$
Standard deviation	$5.6465964334372154 \times 10^{-1}$	$2.5378997817307986 \times 10^{-1}$
Percentage of better cases	18.0	24.2

Table 4
The results of one- and two-sample t-test: t-statistics (t) and p-values (p); all parameters are the same as in Table 3.

	Two-dimensional example	Three-dimensional example
(H_A)	$t = 0.97567$, $p = 0.32946$	$t = 0.02931$, $p = 0.9766$
(H_B)	$t = 1.49326$, $p = 0.13569$	$t = 6.38419$, $p < 10^{-9}$
(H_C)	$t = -1.28787$, $p = 0.19794$	$t = -6.31634$, $p < 10^{-9}$

- The difference between the accuracy of the results obtained using regularly and randomly distributed nodes was statistically significant only in three-dimensional example.
- In three-dimensional example, statistically significant difference between the accuracy of the method with perturbed and randomly distributed nodes was detected, while in two-dimensional example such the difference was statistically insignificant.

If the number of regularly distributed nodes N is increased, the fill distance decreases. From Fig. 9 we see how the increased number of nodes affects the accuracy of the method.

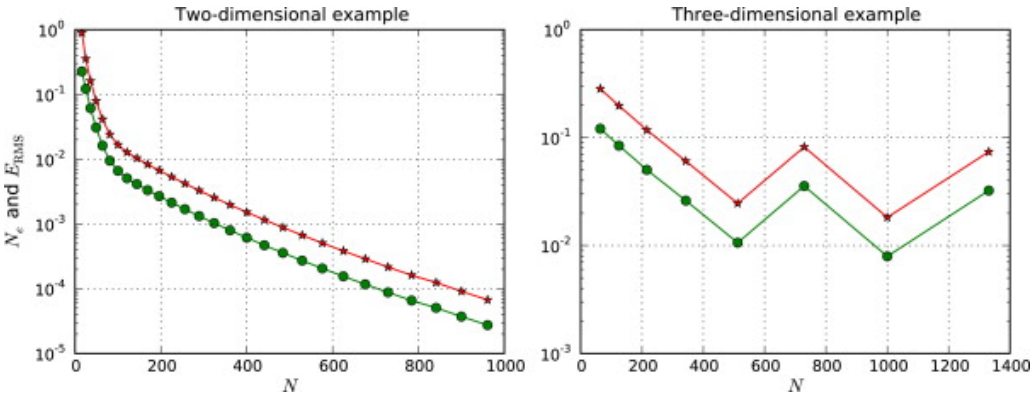

Figure 9: The dependence of the accuracy of the method (errors N_e and E_{RMS} are depicted as red curves with stars and green curves bullets, respectively) on the number of nodes N (nodes are distributed regularly): $\xi = 0.25$ ($\xi_1 = 0.25$, $\xi_2 = 0.75$); $\epsilon = 3.0$ (two-dimensional example) and $\epsilon = 1.75$ (three-dimensional example). (For interpretation of the references to color in this figure legend, the reader is referred to the web version of this article.)

4. Concluding remarks

We examined the RBF-based meshless method for the solution of multidimensional elliptic equation with classical Dirichlet boundary condition and nonlocal integral conditions. The problem is formulated on cylindrical domain. By solving two- and three-dimensional examples with manufactured solutions we have demonstrated that considered method can be efficient for the solution of such type of nonclassical multidimensional problems. The implementation of the RBF-based method for a multidimensional problem usually is as simple as for a one-dimensional problem.

In this paper, we examined standard RBF collocation approach without any improvements. However, the influence of the round-off errors can be eliminated and the accuracy of the technique can be increased significantly if the arbitrary precision arithmetic is utilized for the computation [64, 66, 69]. Regularization techniques also can improve the standard approach [39].

The RBF collocation technique also can be used for the solution of nonlinear elliptic problems (see e. g. [36, 70]). Our next goal is to construct and examine the RBF-based meshless method for the solution of multidimensional nonlinear elliptic equation with nonlocal boundary condition [71].

Acknowledgments

The author is very grateful to the anonymous reviewers for their constructive comments and suggestions which have improved the paper.

References

[1] W. A. Day, Existence of a property of solutions of the heat equation subject to linear thermoelasticity and other theories, Quart. Appl. Math. 40 (1985) 319–30.
[2] W. A. Day, Parabolic equations and thermodynamics, Quart. Appl. Math. 50 (1992) 523–33.
[3] R. Čiupaila, M. Sapagovas, O. Štikonienė, Numerical solution of nonlinear elliptic equation with nonlocal condition, Nonlinear Anal. Model. Control 18 (2013) 412–26.
[4] J. I. Díaz, J. F. Padial, J. M. Rakotoson, Mathematical treatment of the magnetic confinement in a current carrying stellarator, Nonlinear Anal. 34 (1998) 857–87.
[5] G. Avalishvili, M. Avalishvili, D. Gordeziani, On a nonlocal problem with integral boundary conditions for a multidimensional elliptic equation, Appl. Math. Lett. 24 (2011) 566–71.

[6] G. Avalishvili, M. Avalishvili, D. Gordeziani, On integral nonlocal boundary value problems for some partial differential equations, Bull. Georgian Acad. Sci. (N. S.) 5 (2011) 31–7.
[7] G. Berikelashvili, On a nonlocal boundary-value problem for two-dimensional elliptic equation, Comput. Methods Appl. Math. 3 (2003) 35–44.
[8] M. P. Sapagovas, Difference method of increased order of accuracy for the Poisson equation with nonlocal conditions, Differ. Equ. 44 (2008) 1018–28.
[9] M. Sapagovas, O. Štikonienė, A fourth-order alternating-direction method for difference schemes with nonlocal condition, Lith. Math. J. 49 (2009) 309–17.
[10] M. Sapagovas, O. Štikonienė, Alternating-direction method for a mildly nonlinear elliptic equation with nonlocal integral conditions, Nonlinear Anal. Model. Control 16 (2011) 220–30.
[11] M. Sapagovas, A. Štikonas, O. Štikonienė, Alternating direction method for the Poisson equation with variable weight coefficients in an integral condition, Differ. Equ. 47 (2011) 1176–87.
[12] G. Berikelashvili, N. Khomeriki, On the convergence of difference schemes for one nonlocal boundary-value problem, Lith. Math. J. 52 (2012) 353–62.
[13] G. Berikelashvili, N. Khomeriki, On a numerical solution of one nonlocal boundary-value problem with mixed Dirichlet–Neumann conditions, Lith. Math. J. 53 (2013) 367–80.
[14] C. Nie, H. Yu, Some error estimates on the finite element approximation for two-dimensional elliptic problem with nonlocal boundary, Appl. Numer. Math. 68 (2013) 31–8.
[15] C. Nie, S. Shu, H. Yu, Q. An, A high order composite scheme for the second order elliptic problem with nonlocal boundary and its fast algorithm, Appl. Math. Comput. 227 (2014) 212–21.
[16] E. A. Volkov, A. A. Dosiyev, S. C. Buranay, On the solution of a nonlocal problem, Comput. Math. Appl. 66 (2013) 330–8.
[17] N. Gordeziani, P. Natalini, P. E. Ricci, Finite-difference methods for solution of nonlocal boundary value problems, Comput. Math. Appl. 50 (2005) 1333–44.
[18] A. Ashyralyev, E. Ozturk, The numerical solution of the Bitsadze-Samarskii nonlocal boundary value problems with the Dirichlet-Neumann condition, Abstr. Appl. Anal. 2012 (2012) 13 pages, Article ID 730804.
[19] A. Ashyralyev, F. S. O. Tetikoglu, FDM for elliptic equations with Bitsadze-Samarskii-Dirichlet conditions, Abstr. Appl. Anal. 2012 (2012) 22 pages, Article ID 454831.
[20] G. R. Liu, Meshfree Methods: Moving Beyond the Finite Element Method, second ed., CRC Press, 2009.
[21] H. Li, S. S. Mulay, Meshless Methods and Their Numerical Properties, CRC Press, 2013.
[22] M. D. Buhmann, Radial Basis Functions: Theory and Implementations, volume 12 of *Cambridge Monographs on Applied and Computational Mathematics*, Cambridge University Press, 2003.
[23] H. Wendland, Scattered Data Approximation, volume 17 of *Cambridge Monographs on Applied and Computational Mathematics*, Cambridge University Press, 2005.
[24] S. A. Sarra, E. J. Kansa, Multiquadric Radial Basis Function Approximation Methods for the Numerical Solution of Partial Differential Equations, volume 2 of *Advances in Computational Mechanics*, Tech Science Press, 2009.
[25] E. J. Kansa, Multiquadrics—A scattered data approximation scheme with applications to computational fluid-dynamics—II solutions to parabolic, hyperbolic and elliptic partial differential equations, Comput. Math. Appl. 19 (1990) 147–61.
[26] I. Boztosun, A. Charafi, An analysis of the linear advection–diffusion equation using mesh-free and mesh-dependent methods, Eng. Anal. Bound. Elem. 26 (2002) 889–95.
[27] E. Larsson, B. Fornberg, A numerical study of some radial basis function based solution methods for elliptic PDEs, Comput. Math. Appl. 46 (2003) 891–902.
[28] J. Li, A. H.-D. Cheng, C.-S. Chen, A comparison of efficiency and error convergence of multiquadric collocation method and finite element method, Eng. Anal. Bound. Elem. 27 (2003) 251–7.
[29] M. Sharan, E. J. Kansa, S. Gupta, Application of the multiquadric method for numerical solution of elliptic partial differential equations, Appl. Math. Comput. 84 (1997) 275–302.
[30] E. J. Kansa, Y. C. Hon, Circumventing the ill-conditioning problem with multiquadric radial basis functions: Applications to elliptic partial differential equations, Comput. Math. Appl. 39 (2000) 123–37.
[31] A. I. Fedoseyev, M. J. Friedman, E. J. Kansa, Improved multiquadric method for elliptic partial differential equations via PDE collocation on the boundary, Comput. Math. Appl. 43 (2002) 439–55.
[32] L. Jianyu, L. Siwei, Q. Yingjian, H. Yaping, Numerical solution of elliptic partial differential equation using radial basis function neural networks, Neural Netw. 16 (2003) 729–34.
[33] H.-Y. Hu, Z.-C. Li, A. H.-D. Cheng, Radial basis collocation methods for elliptic boundary value problem, Comput. Math. Appl. 50 (2005) 289–320.
[34] H.-Y. Hu, Z.-C. Li, Collocation methods for Poisson's equation, Comput. Methods Appl. Mech. Engrg. 195 (2006) 4139–60.
[35] J. Wertz, E. J. Kansa, L. Ling, The role of the multiquadric shape parameters in solving elliptic partial differential equations, Comput. Math. Appl. 51 (2006) 1335–48.

[36] H. Y. Hu, J. S. Chen, Radial basis collocation method and quasi-Newton iteration for nonlinear elliptic problems, Numer. Methods Partial Differential Equations 24 (2008) 991–1017.
[37] N. Mai-Duy, T. Tran-Cong, A multidomain integrated-radial-basis-function collocation method for elliptic problems, Numer. Methods Partial Differential Equations 24 (2008) 1301–20.
[38] H.-D. Huang, H.-D. Yen, A. H.-D. Cheng, On the increasingly flat radial basis function and optimal shape parameter for the solution of elliptic PDEs, Eng. Anal. Bound. Elem. 34 (2010) 802–9.
[39] J. Lin, W. Chen, K. Y. Sze, A new radial basis function for Helmholtz problems, Eng. Anal. Bound. Elem. 36 (2012) 1923–30.
[40] A. Bouhamidi, M. Hached, K. Jbilou, A meshless method for the numerical computation of the solution of steady Burgers-type equations, Appl. Numer. Math. 74 (2013) 95–110.
[41] Z. Liu, Y. He, Solving the elliptic Monge–Ampère equation by Kansa's method, Eng. Anal. Bound. Elem. 37 (2013) 84–8.
[42] Z. Liu, Y. He, Cascadic meshfree method for the elliptic Monge–Ampère equation, Eng. Anal. Bound. Elem. 37 (2013) 990–6.
[43] Z. Liu, Y. He, An iterative meshfree method for the elliptic Monge–Ampère equation in 2D, Numer. Methods Partial Differential Equations (2013) in press, doi: 10.1002/num.21849.
[44] M. Dehghan, M. Tatari, Use of radial basis functions for solving the second-order parabolic equation with nonlocal boundary conditions, Numer. Methods Partial Differential Equations 24 (2008) 924–38.
[45] M. Dehghan, M. Tatari, On the solution of the non-local parabolic partial differential equations via radial basis functions, Appl. Math. Model. 33 (2009) 1729–38.
[46] M. Dehghan, A. Shokri, A meshless method for numerical solution of the one-dimensional wave equation with an integral conditions using radial basis functions, Numer. Algorithms 52 (2009) 461–77.
[47] S. Kazem, J. A. Rad, Radial basis functions method for solving of a non-local boundary value problem with Neumann's boundary conditions, Appl. Math. Model. 36 (2012) 2360–9.
[48] S. Sajavičius, Optimization, conditioning and accuracy of radial basis function method for partial differential equations with nonlocal boundary conditions—A case of two-dimensional Poisson equation, Eng. Anal. Bound. Elem. 37 (2013) 788–804.
[49] R. Schaback, Error estimates and condition numbers for radial basis function interpolation, Adv. Comput. Math. 3 (1995) 251–64.
[50] W. R. Madych, S. A. Nelson, Bounds on multivariate interpolation and exponential error estimates for multiquadric interpolation, J. Approx. Theory 70 (1992) 94–114.
[51] W. R. Madych, Miscellaneous error bounds for multiquadric and related interpolators, Comput. Math. Appl. 24 (1992) 121–38.
[52] E. Jones, T. Oliphant, P. Peterson, et al., SciPy: Open source scientific tools for Python, 2001. URL: http://www.scipy.org/.
[53] SciPy Reference Guide, Release 0.13.0, 2013.
[54] R. L. Hardy, Multiquadric equations of topography and other irregular surfaces, J. Geophys. Res. 76 (1971) 1905–15.
[55] R. Franke, Scattered data interpolation: tests of some methods, Math. Comp. 38 (1982) 181–200.
[56] R. E. Carlson, T. A. Foley, The parameter r^2 in multiquadric interpolation, Comput. Math. Appl. 21 (1991) 29–42.
[57] T. A. Foley, Near optimal parameter selection for multiquadric interpolation, J. Appl. Sci. Comput. 1 (1994) 54–69.
[58] S. Rippa, An algorithm for selecting a good value for the parameter c in radial basis function interpolation, Adv. Comput. Math. 11 (1999) 193–210.
[59] C. J. Trahan, R. E. Wyatt, Radial basis function interpolation in the quantum trajectory method: optimization of the multiquadric shape parameter, J. Comput. Phys. 185 (2003) 27–49.
[60] G. E. Fasshauer, J. G. Zhang, On choosing "optimal" shape parameters for RBF approximation, Numer. Algorithms 45 (2007) 345–68.
[61] M. Scheuerer, An alternative procedure for selecting a good value for the parameter c in RBF-interpolation, Adv. Comput. Math. 34 (2011) 105–26.
[62] M. Uddin, On the selection of a good value of shape parameter in solving time-dependent partial differential equations using RBF approximation method, Appl. Math. Model. 38 (2014) 135–44.
[63] A. H.-D. Cheng, M. A. Golberg, E. J. Kansa, G. Zammito, Exponential convergence and h-c multiquadric collocation method for partial differential equations, Numer. Methods Partial Differential Equations 19 (2003) 571–94.
[64] C.-S. Huang, C.-F. Lee, A. H.-D. Cheng, Error estimate, optimal shape factor, and high precision computation of multiquadric collocation method, Eng. Anal. Bound. Elem. 31 (2007) 614–23.
[65] C. M. C. Roque, A. J. M. Ferreira, Numerical experiments on optimal shape parameters for radial basis functions, Numer. Methods Partial Differential Equations 26 (2010) 675–89.
[66] A. H.-D. Cheng, Multiquadric and its shape parameter—A numerical investigation of error estimate, condition number, and round-off error by arbitrary precision computation, Eng. Anal. Bound. Elem. 36 (2012) 220–39.

[67] J. P. Boyd, K. W. Gildersleeve, Numerical experiments on the condition number of the interpolation matrices for radial basis functions, Appl. Numer. Math. 61 (2011) 443–59.
[68] Y. Duan, Y. C. Hon, W. Zhao, Stability estimate on meshless unsymmetric collocation method for solving boundary value problems, Eng. Anal. Bound. Elem. 37 (2013) 666–72.
[69] S. A. Sarra, Radial basis function approximation methods with extended precision floating point arithmetic, Eng. Anal. Bound. Elem. 35 (2011) 68–76.
[70] G. E. Fasshauer, Newton iteration with multiquadrics for the solution of nonlinear PDEs, Comput. Math. Appl. 43 (2002) 423–38.
[71] Y. Wang, Solutions to nonlinear elliptic equations with a nonlocal boundary condition, Electron. J. Differential Equations 2002 (2002) 16 pages, No. 05.